

## Supporting Information

### Enhanced thermoelectric performance of GeTe through *in situ* micro domain and Ge vacancy control

**Khasim Saheb Bayikadi<sup>a</sup>, Raman Sankar<sup>\*a,b</sup>, Chien Ting Wu<sup>c</sup>, Chengliang Xia<sup>f</sup>, Yue Chen<sup>f</sup>, Li-Chyong Chen<sup>b,d</sup>, Kuei-Hsien Chen<sup>\*b,c</sup>, Fang-Cheng Chou<sup>\*b,d</sup>**

<sup>a</sup> Institute of Physics, Academia Sinica, Nankang, Taipei, R.O.C. Taiwan 11529.

<sup>b</sup> Centre for Condensed Matter Sciences, National Taiwan University, Taipei 106, Taiwan.

<sup>c</sup> Institute of Atomic and Molecular Sciences, Academia Sinica, Taipei 106, Taiwan.

<sup>d</sup> Center of Atomic Initiative for New Materials, National Taiwan University, Taipei 10617, Taiwan

<sup>e</sup> Taiwan Semiconductor Research Institute, Hsinchu Science Park, Hsinchu 300, Taiwan, R.O.C.

<sup>f</sup> Department of Mechanical Engineering, The University of Hong Kong, Pokfulam Road, Hong Kong SAR, China

**\*Corresponding Author: [sankarraman@gate.sinica.edu.tw](mailto:sankarraman@gate.sinica.edu.tw) (R Sankar),  
[chenkh@pub.iams.sinica.edu.tw](mailto:chenkh@pub.iams.sinica.edu.tw) (K H Chen), [fcchou@ntu.edu.tw](mailto:fcchou@ntu.edu.tw) (F C Chou)**

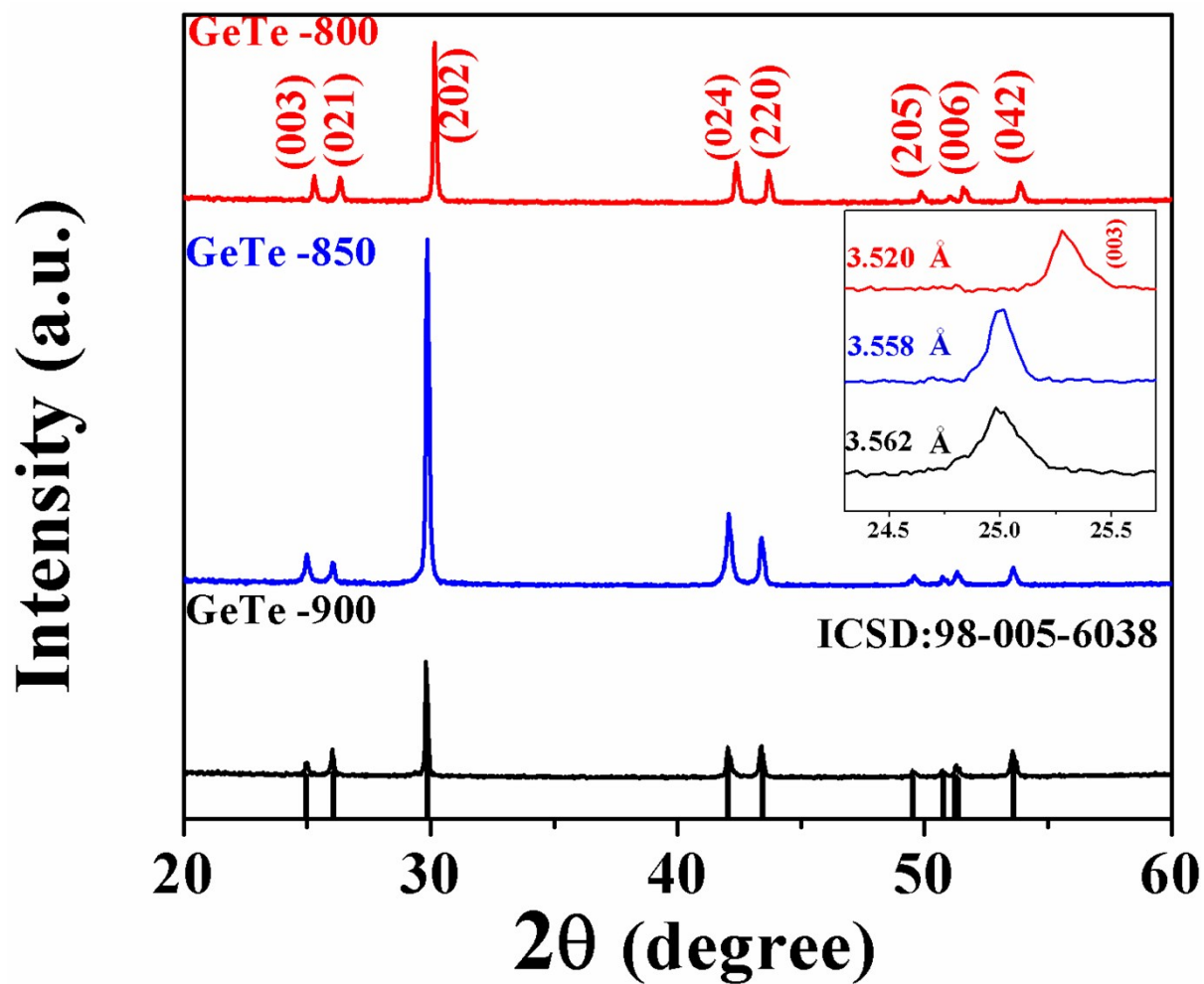


Figure S1: XRD patterns for the GeTe sample series quenched at different temperatures. (003) peak is found shifted toward smaller angle to indicate increased inter-layer distance among Ge-Te layer along the c-direction of R3m symmetry, which is presumably related to factors including strain, Ge vacancy level, and interstitials between layers.

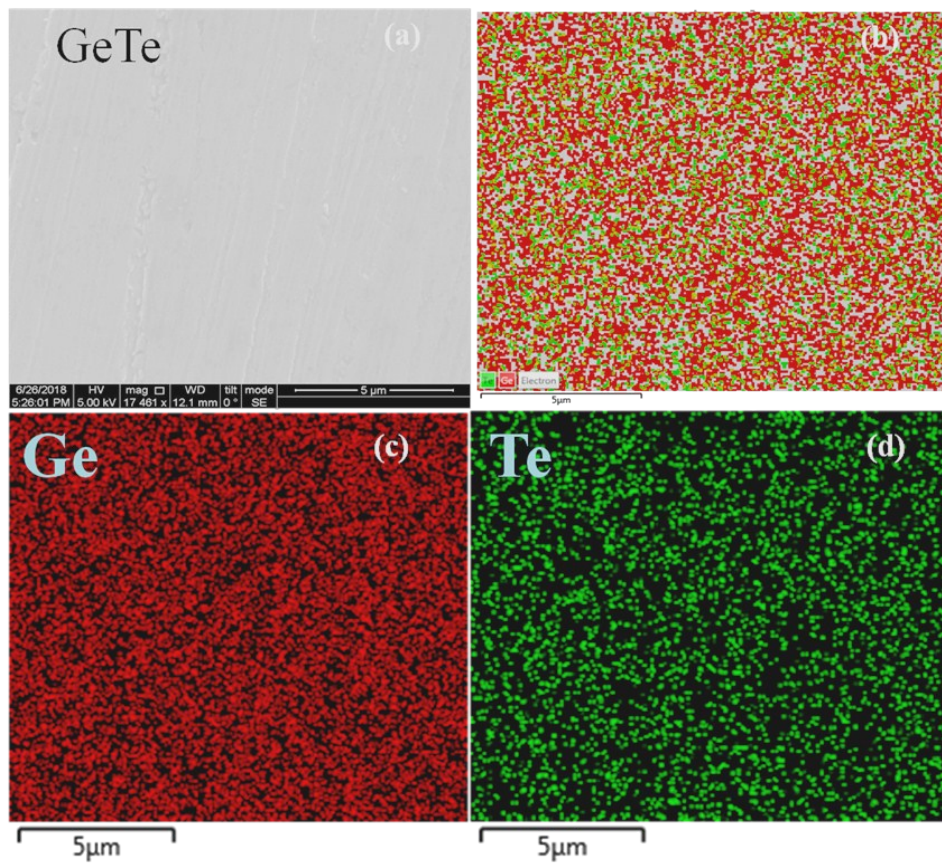


Figure S2: (a) FE-SEM image of hot pressed pellet of GeTe-900. (b) Elemental mapping of the surface, (c) Ge mapping, and (d) Te mapping. Elemental mapping analysis implies there are no Ge precipitants in GeTe-900 sample.

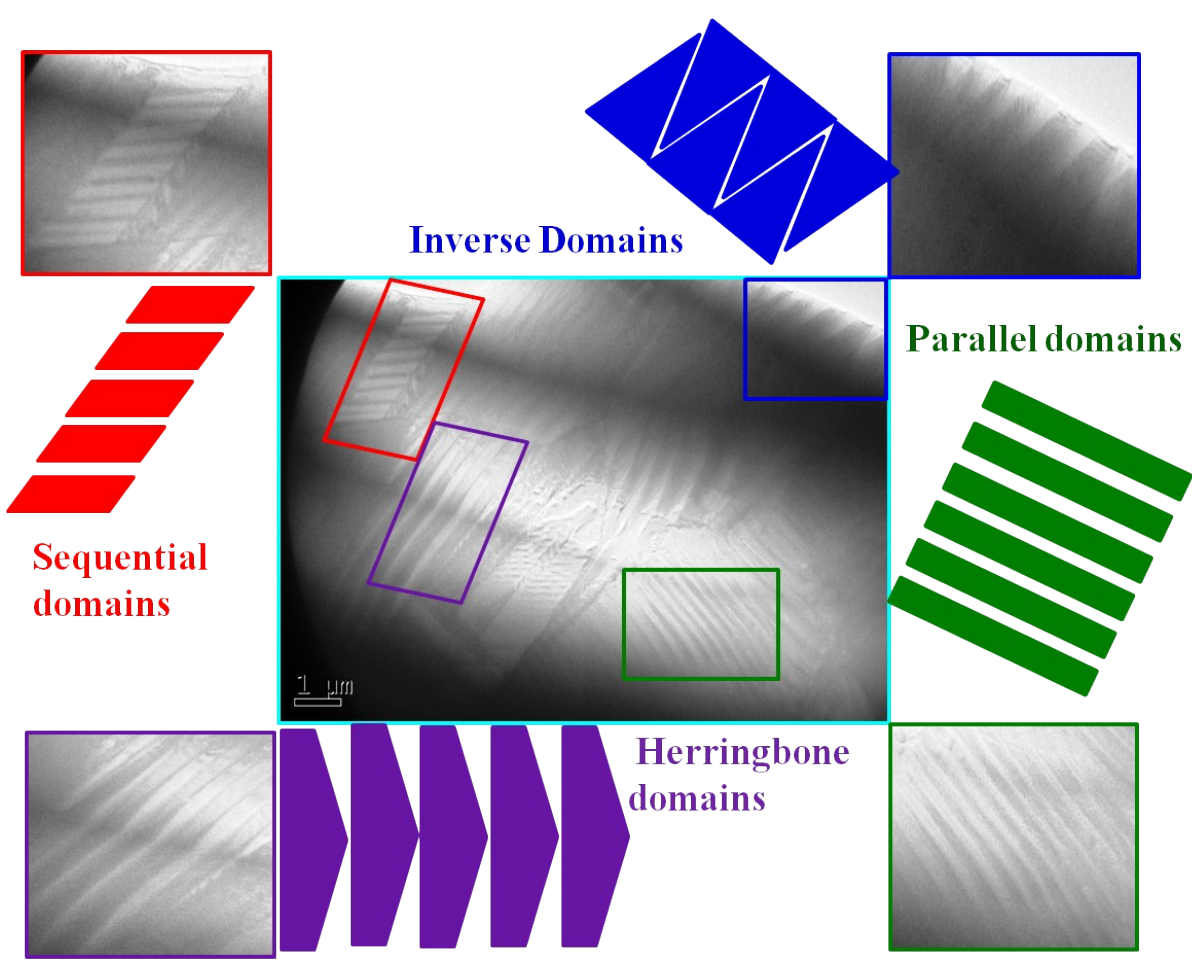


Figure S3: Various micro domain images of GeTe-900, including the typical herringbone structure micro domains, random domains, and twin domains in different contrasts and orientations.

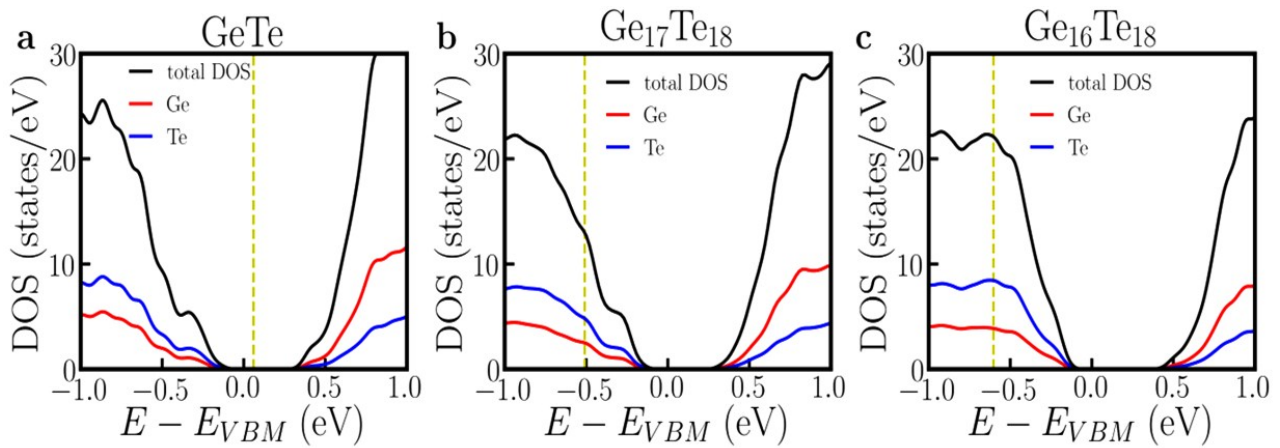


Figure S4: Calculated electronic density of states for the Ge<sub>18</sub>Te<sub>18</sub>, Ge<sub>17</sub>Te<sub>18</sub> and Ge<sub>16</sub>Te<sub>18</sub>, along with its partial DOS for the individual Ge and Te in all compositions.

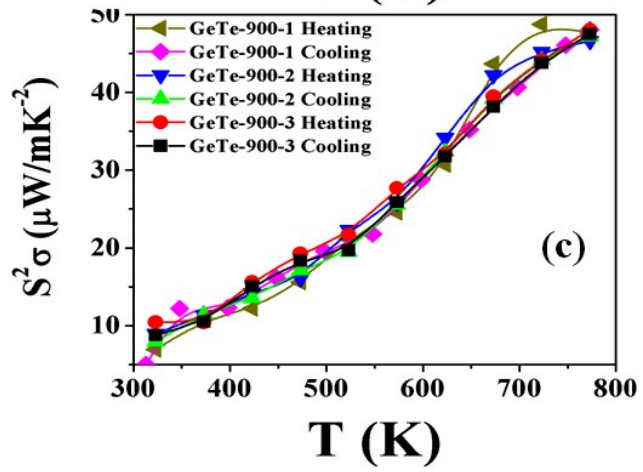
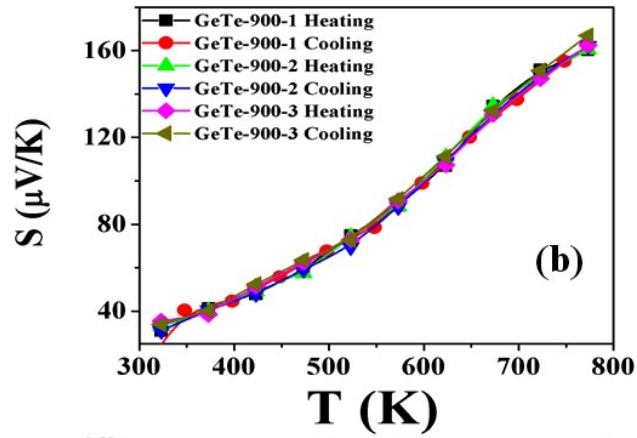
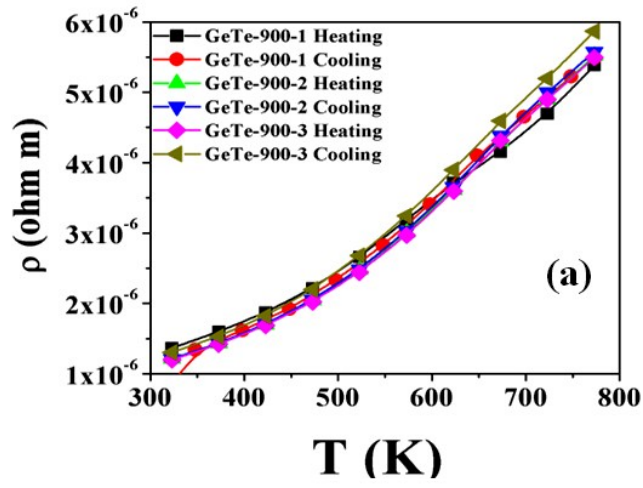


Figure S5: Reproducibility of thermoelectric properties is verified with three batches of sample from the pure element precursors, including heating and cooling cycles for the (a) resistivity, (b) Seebeck Coefficient, and (c) power factor measurements.

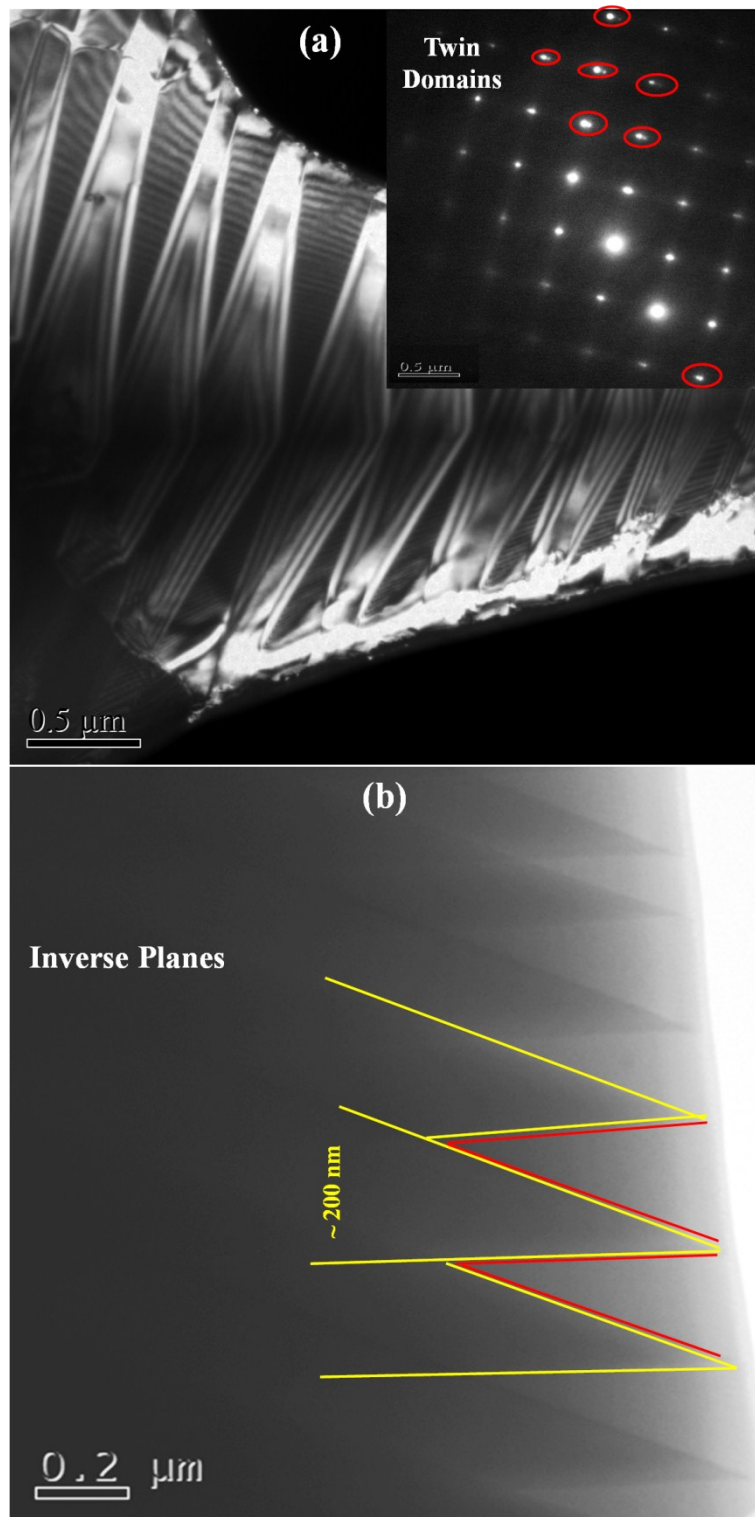


Figure S6: (a) Twin domains of the GeTe-900 (Inset: SAED pattern of the twin domains), and (b) Inverse domains of GeTe-900 with size varying from few nm to  $\sim 200 \text{ nm}$ .

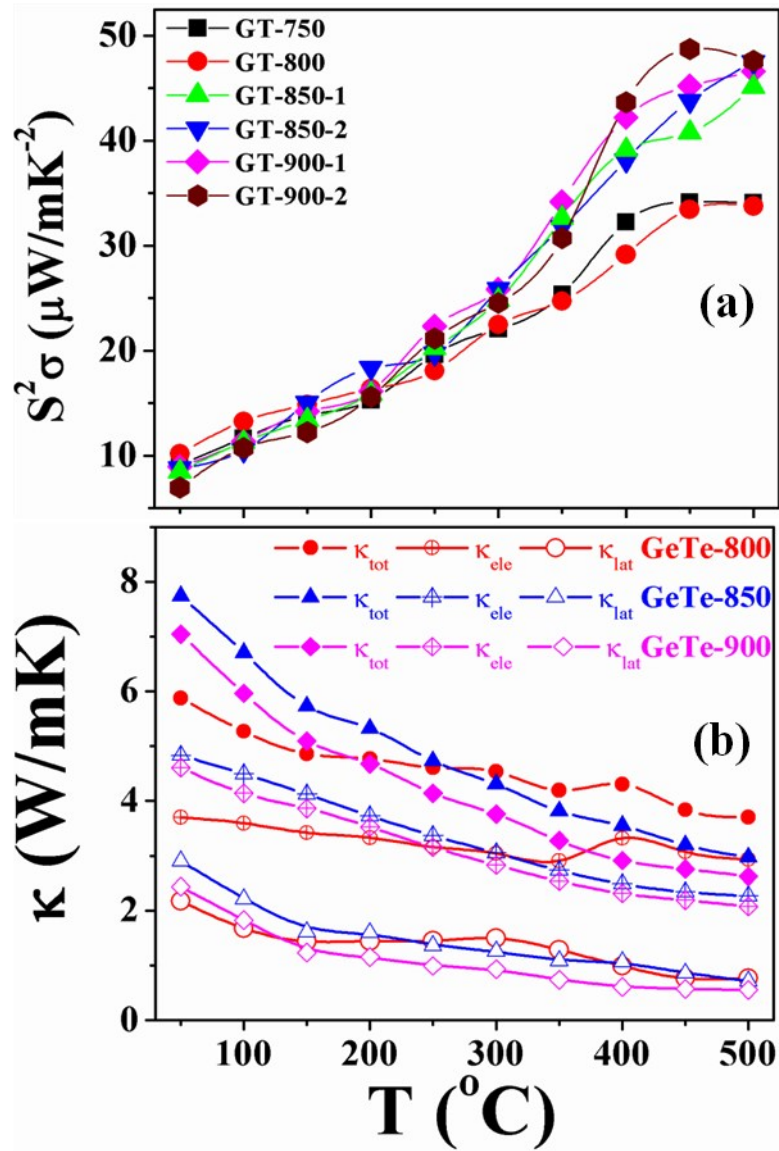


Figure S7: Temperature dependence for GeTe of various Ge vacancy levels and micro domain structures, (a) power factor and (b) Thermal conductivity ( $\kappa_{\text{tot}}$ ,  $\kappa_{\text{lat}}$  &  $\kappa_{\text{ele}}$ ).